

Semantic Guided Large Scale Factor Remote Sensing Image Super-resolution with Generative Diffusion Prior

Ce Wang, Wanjie Sun*

School of Remote Sensing and Information Engineering, Wuhan University
Wuhan 430079, China

{cewang, sunwanjie}@whu.edu.cn

Abstract

Remote sensing images captured by different platforms exhibit significant disparities in spatial resolution. Large scale factor super-resolution (SR) algorithms are vital for maximizing the utilization of low-resolution (LR) satellite data captured from orbit. However, existing methods confront challenges in recovering SR images with clear textures and correct ground objects. We introduce a novel framework, the Semantic Guided Diffusion Model (SGDM), designed for large scale factor remote sensing image super-resolution. The framework exploits a pre-trained generative model as a prior to generate perceptually plausible SR images. We further enhance the reconstruction by incorporating vector maps, which carry structural and semantic cues. Moreover, pixel-level inconsistencies in paired remote sensing images, stemming from sensor-specific imaging characteristics, may hinder the convergence of the model and diversity in generated results. To address this problem, we propose to extract the sensor-specific imaging characteristics and model the distribution of them, allowing diverse SR images generation based on imaging characteristics provided by reference images or sampled from the imaging characteristic probability distributions. To validate and evaluate our approach, we create the Cross-Modal Super-Resolution Dataset (CMSRD). Qualitative and quantitative experiments on CMSRD showcase the superiority and broad applicability of our method. Experimental results on downstream vision tasks also demonstrate the utilitarian of the generated SR images. The dataset and code will be publicly available at <https://github.com/wwangcece/SGDM>

1. Introduction

High-resolution (HR) remote sensing imagery is crucial in various applications, such as weather prediction [45], agricultural crop type identification [39], geographic object de-

tection [21], and land use/cover mapping [43, 61]. However, accessing HR images is often challenging due to limited satellite coverage, high costs, infrequent revisit times, reduced spectral resolution, and sensitivity to weather conditions [1, 26]. In contrast, satellites with lower spatial resolution offer wider coverage, more frequent revisit, and better cost-effectiveness, but they lack critical details for precise object identification or monitoring. Consequently, there is a strong demand for software-based algorithms to enhance low-resolution (LR) images, providing an efficient and cost-effective means to leverage globally available LR remote sensing data.

Image super-resolution (SR) aims to reconstruct higher-resolution images with enhanced details from LR sources, enabling the acquisition of HR images beyond the sampling constraints of digital imaging systems. As a result, algorithmic SR methods have become a prominent research topic in computer vision and image processing. Over the past decades, various SR approaches have been developed, including reconstruction-based [40], example-based [10], sparse representation-based [55], and regression-based [42] approaches. With the advancement of deep learning techniques, deep neural network-based SR models have significantly outperformed traditional interpolation and optimization techniques. Early deep learning research in SR focused on the design of network architectures [7, 19], loss function [3, 15], and optimization strategy [28, 51], leading to notable improvements in fidelity-oriented quantitative performance. Recently, generative models like variational autoencoders [30], generative adversarial networks [50], normalizing flows [31], and diffusion models [37] have showcased impressive perceptual quality in SR results.

Previous research on SR in both natural and remote sensing images has predominantly focused on small scale factors, like $2\times$ or $4\times$. However, in real-world scenarios, there is often a significant disparity in spatial resolution between different remote sensing platforms. For instance, Landsat series satellites have a spatial resolution of approximately 80 meters in the visible and near-infrared bands, Sentinel

series satellites have a spatial resolution of about 10 meters, and WorldView-3 satellites achieve a spatial resolution of 1.24 meters. Consequently, large scale factor SR models are essential to leverage LR satellite images for specific applications. However, large scale factor SR poses significant challenges due to the severe loss of detailed information in LR images, making SR a highly ill-posed problem with a vast solution space. To address this, researchers often employ prior knowledge from natural HR images to restrict SR results to a low-dimensional manifold. Commonly used priors include statistical models [38], sparse representation [55], and low-rank structures [41].

Recently, learning-based priors based on pre-trained neural networks, like PULSE [33] and GLEAN [4], have shown remarkable performance in large scale factor SR. The Stable Diffusion model, trained on billions of text-image pairs, has been employed as a generative prior in image restoration tasks, significantly enhancing visual quality by producing natural-looking, high-quality images [29, 49, 57]. Nonetheless, employing a generative prior for large scale factor SR often leads to the hallucination of image details that do not align with the ground truth. As a result, harnessing pre-trained generative diffusion models as natural HR priors for generating remote sensing images with accurate structures and realistic textures remains a challenging task.

In Fig. 1, we showcase two pairs of LR and HR remote sensing images from a real-world scenario. The LR images are captured by Sentinel-2, with a resolution of 10 meters, while the HR images are sourced from the World Imagery, with a spatial resolution of 1.07 meters. The main challenges in large scale factor SR in real-world contexts stem from the significant difference between LR and HR images, including:

- Difficulty in recovering semantically accurate and texture clear results. Due to the loss of most high-frequency information in LR images, it is challenging to reconstruct perceptually plausible and semantically correct HR images from LR images even with the state-of-the-art generative methods.
- Instability in model training due to pixel misalignment between LR and HR images. Due to the differences in imaging characteristics among different sensors, LR and HR images are aligned only at the semantic level rather than pixel level, posing significant challenges for stable model training.

To circumvent the aforementioned issues, we propose a new framework named Semantic Guided Diffusion Model (SGDM) for large scale factor remote sensing image super-resolution. SGDM utilizes the pre-trained Stable Diffusion model to generate SR results with more realistic textures. However, relying solely on pre-trained generative models as a prior cannot produce structural and semantic accurate

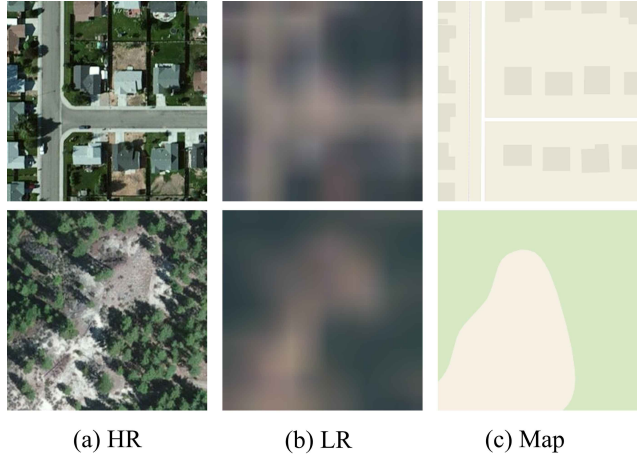


Figure 1. In real-world scenarios, there exists a significant spatial resolution disparity among remote-sensing images captured by different sensors. Vector maps, on the other hand, provide rich semantic guidance for large scale factor super-resolution.

ground objects when SR factor is large. Fortunately, vector maps, which are readily available, provide strong semantic guidance for large scale factor SR tasks. Our proposed SGDM can effectively exploit vector maps for enhanced fidelity in the SR process. Furthermore, to accommodate the differences in imaging characteristics across various sensors in real-world scenarios, we propose a method to implicitly decouple imaging characteristics from image content, enabling probabilistic modeling of the imaging characteristics. Finally, we also introduce a new dataset, the Cross-Modal Super-Resolution Dataset (CMSRD), to validate and evaluate the proposed SGDM. Experimental results demonstrate that our method outperforms existing state-of-the-art (SOTA) methods in quantitative metrics and achieves greater flexibility and visual style control. Experimental results on downstream vision tasks, such as semantic segmentation and scene recognition, also demonstrate the effectiveness of the proposed SGDM and the usability of the generated SR results.

The main contributions of this work are summarized as follows:

- A novel remote sensing image super-resolution framework, named Semantic Guided Diffusion Model is proposed. It can achieve up to $32\times$ super-resolution with accurate structures and realistic textures.
- We propose to incorporate vector maps into the super-resolution process, and validate its effectiveness for large scale factor super-resolution tasks by providing structural and semantic cues.
- We propose to decouple imaging characteristics from image content, addressing pixel-level inconsistencies between LR and HR images, and achieve diverse SR results

generation with either imaging characteristics guidance or sampling.

- We provide an open-sourced Cross-Modal Super-Resolution Dataset (CMSRD), which contains 45300 pairs of synthetic LR/HR images and 50754 pairs real-world LR/HR images, to evaluate the proposed SGDM and facilitate the future research on large scale factor remote sensing image super-resolution for the community.

The remainder of this paper is organized as follows. Section 2 reviews the work of remote sensing image super-resolution and large scale factor image super-resolution. In Section 3, we introduce the details of our method, including the main idea and the specific architecture of the semantic guided diffusion model. Section 4 introduces the data and evaluation metrics of this work. We present experimental results and ablation studies in Section 5 and Section 6. And finally, Section 7 presents our conclusions.

2. Related work

2.1. Remote sensing image super-resolution

In recent years, the rapid advancement of deep learning has led to the emergence of numerous deep learning-based super-resolution (SR) methods, showcasing their superiority over traditional techniques. These methods could be categorized into four main types: PSNR-oriented, GAN-based, flow-based, and diffusion-based methods. PSNR-oriented models [7, 28, 67] are trained using straightforward loss functions (e.g., L1 or L2 loss), resulting in impressive PSNR scores. However, these loss functions tend to guide the SR results towards an average of several potential predictions, leading to over-smoothing images and the loss of high-frequency information. GAN-based approaches [20, 50, 63] address this issue by incorporating content (L1 or L2) and adversarial losses, enhancing perceptual quality but may struggle with convergence and mode collapse. Flow-based methods [25, 31] use invertible encoders to tackle the ill-posed problem, but face high training costs due to strict architectural requirements. Recently, denoising diffusion probabilistic models (DDPM) [13] have received increasing attention in the realm of image-to-image translation [56], and also achieved promising performance in super-resolution tasks [22]. SR3 [37] is the first to adapt DDPM for SISR tasks, yielding competitive perceptual quality. Although DDPM-based methods can model more intricate distributions and alleviate the training instability which are often encountered in GANs, these methods all involve training the diffusion models from scratch, which demands substantial computational resources and carries the potential risk of compromising the generative priors captured in generative models [49].

Due to the rapid advancement of deep learning, deep learning-based remote sensing image SR research has also

advanced. [27] was among the first to employ convolution neural networks for this task, outperforming traditional methods in upscaling Sentinel-2 images. Subsequently, studies on remote sensing image SR have primarily focused on two directions. The first direction involves designing specialized models for remote sensing images. Taking into account the complex edge details commonly found in remote sensing images, [58] devised an edge enhancement network and introduced edge loss. In light of much more complex structure of remote sensing images than that of natural images, [66] proposed a scene-adaptive super-resolution strategy to more accurately describe the structural features of different scenes. In addition to improvements in super-resolution models, another direction aims to bridge the gap between synthetic and real-world imagery. For instance, [69] proposed a realistic training data generation model for commercial satellite imagery products and [35] focused on enhancing the spatial resolution of Sentinel-2 satellite images using very high-resolution (VHR) PeruSat-1 images as a reference set.

Recently, the pre-trained Stable Diffusion model [36] has demonstrated success in content generation [64]. As a result, there is growing interest in leveraging pre-trained models for super-resolution tasks [29, 49, 57]. However, due to the distinct nature of remote sensing imagery, there has been limited exploration of integrating the pre-trained Stable Diffusion model into remote sensing image super-resolution. Despite this, the potential of the pre-trained model in this field remains substantial.

2.2. Large scale factor image super-resolution

Due to the highly ill-posed nature of large scale factor super-resolution, many methods require additional prior information to achieve better outcomes. Methods based on explicit priors rely on additional inputs to provide more realistic texture or semantic guidance, such as reference images [41, 68], semantic masks [2], hyperspectral data [32], land cover change masks [9], etc. By aligning the input LR images and reference information in the feature space, these methods exploit the reference information to enhance super-resolution. However, acquiring high-quality references and precise feature alignment can be challenging in real-world situations, prompting researchers to explore implicit prior-based methods.

These methods typically utilize pre-trained GAN models to generate more realistic textures. [33] introduced an unsupervised super-resolution approach based on pre-trained GANs, exploring the manifold of natural images to find HR images most similar to the LR input. [11] employed multiple initial latent codes to generate intermediate feature maps and then compose them through channel attention mechanisms. In contrast to previous GAN inversion methods, [4] leveraged pre-trained StyleGAN [16, 17] model

and achieved visually pleasing reconstruction results with a single forward pass. However, such methods can only reconstruct images for specific categories (such as faces, cats, bedrooms, etc.) and struggle to generalize to generic scenes.

In contrast to existing methods, our approach integrates both explicit priors (vector maps) and implicit priors (pre-trained Stable Diffusion model) to generate more realistic textures while maintaining semantic accuracy of the reconstructed results.

3. Methodology

3.1. Main idea

The main idea of our work is illustrated in Fig. 2. Traditionally, generative models for super-resolution only take LR images as input to produce SR images, which can be mathematically expressed as:

$$y = \arg \min_y -\log(p(y|x)) \quad (1)$$

where x represents the LR image, y represents the estimated SR image. $p(\cdot|x)$ is the conditional probability density function of HR images given LR inputs, which is usually modelled as the standard Gaussian (L2 loss) or Laplacian (L1 loss) distribution with the ground truth HR images as mean. Theoretically, this modeling approach that relies solely on LR images can learn the many-to-one mapping between LR and HR images. However, these methods often struggle to obtain sufficiently accurate semantic information about ground objects when the SR factor is large. Additionally, the differences in imaging characteristics among different sensors can hinder the model from converging to its optimal state, resulting in the model to produce the mean value of all possible SR results.

Considering the issues mentioned above and inspired by research on disentangled representation learning, our work proposes the following modeling approach:

$$y = \arg \min_y -\log(p(y|x, con, sty)) \quad (2)$$

where con and sty represent the content condition and style condition respectively. In our work, the terms ‘content’ and ‘style’ have the following definitions: the content component of an image refers to its semantics, which represents the structure of ground objects within the image, whereas the style component refers to a representation of the sensor-specific imaging characteristics. Any useful prior can be used to provide content guidance during training, and diverse reconstruction results can be obtained through style guidance or style sampling during testing. By decomposing the image into content and style components, this modeling approach enables better guidance of the reconstruction results with higher fidelity and plausible diversity.

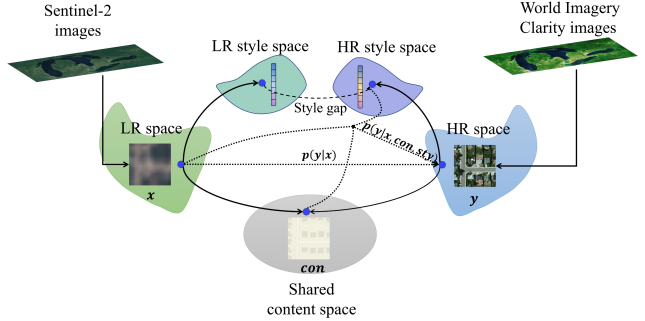


Figure 2. Main idea of our work. Unlike traditional super-resolution methods that only use LR, our approach additionally incorporates content conditions and style conditions. Content guidance can be provided by vector maps, while style guidance can be achieved through style-guided images or style sampling from HR style space.

3.2. Framework overview

3.2.1 Preliminary: diffusion model

Denoising Diffusion Probabilistic Models (DDPM) are a class of generative models based on the diffusion process. The core idea of DDPM is to simulate the diffusion process of data by gradually adding noise and then progressively removing the noise to create new data samples [60]. These two processes are referred to as forward diffusion and reverse denoising, which correspond to the training and sampling procedures of the model. The classic DDPM executes forward diffusion and reverse denoising processes across the entire pixel space with the diffusion process mathematically described as:

$$y_t = \sqrt{\bar{\alpha}_t}y_0 + \sqrt{1 - \bar{\alpha}_t}\epsilon, \quad \epsilon \sim N(0, 1) \quad (3)$$

where y_0 denotes images sampled from the true data distribution, $\bar{\alpha}_t$ represents a pre-set hyperparameter related to noise patterns. The term ϵ refers to random noise drawn from a standard Gaussian distribution. DDPM then focuses on training a denoiser function, ϵ_θ , which aims to estimate the noise added to y_t , subject to an L_2 loss constraint:

$$L = \mathbb{E}_{(y_0, \epsilon, t)} \|\epsilon - \epsilon_\theta(y_t, t)\|^2 \quad (4)$$

where t represents an integer timestamp sampled from the interval $[0, T]$ and ϵ_θ is the noise predictor that we need to train. Following the optimization of the model based on Equation 4, high-quality images can be produced by sequentially refining random noise through the denoising process. If we want to control the generation process more precisely, additional conditional variables can be added to the noise predictor, *i.e.*, $\epsilon_\theta(y_t, t, c)$ in Equation 4. In accordance with the principles of DDPM, each step of this

denoising process can be mathematically described as:

$$y_{t-1} = \frac{1}{\sqrt{\alpha_t}} \left(y_t - \frac{\beta_t}{\sqrt{1-\alpha_t}} \epsilon_\theta \right) + \sigma_t \epsilon, \quad \epsilon \sim N(0, 1) \quad (5)$$

where α_t , $\bar{\alpha}_t$, β_t , and σ_t are hyperparameters related to noise patterns, and ϵ represents additive noise added during the inverse process. After iterating $T - 1$ times, we can obtain the results sampled under the condition c .

However, classical DDPMs often demand substantial computational resources and time for both training and inference, limiting their broader application. In contrast, latent diffusion models shift the diffusion and denoising steps from pixel space to the latent space of a pre-trained autoencoder with much smaller spatial resolution. The encoding and decoding processes of the autoencoder can be expressed as follows:

$$z_0 = \mathcal{E}(y) \quad (6)$$

$$y \approx \mathcal{D}(z_0) \quad (7)$$

where z_0 denotes the latent representation of the HR image y , \mathcal{E} denotes the pre-trained encoder, and \mathcal{D} represents the pre-trained decoder. Then the entire diffusion and denoising process will subsequently take place in the latent space where z_0 resides, thereby achieving an optimal balance between reducing complexity and preserving details.

3.2.2 Semantic guided diffusion model

Based on the discussion of challenges in large scale factor super-resolution of remote sensing images in real-world scenarios, we propose a new super-resolution framework called Semantic Guided Diffusion Model (SGDM). The main structure of the SGDM is shown in Fig. 3. Unlike previous single-image super-resolution frameworks, SGDM can simultaneously accept inputs of LR images, high-resolution style guidance images, and vector maps to jointly reconstruct HR images.

The entire framework of the SGDM can be divided into four parts: a pre-trained variational autoencoder (VAE), a denoising U-shaped network (U-Net) with skip connections, a content-style encoder (CS-Encoder), and an adapter. The VAE is used to encode and decode HR images, thereby moving the diffusion and denoising processes of classical DDPM from the pixel space to the latent space, which enhances the stability of the training process and reduces computational resource consumption. The U-Net is a conditional noise predictor that iteratively predicts noise to obtain noise-free data. It consists of several encoding layers, middle layers, and decoding layers, most of which are composed of residual modules, cross-attention modules, and self-attention modules. The content-style encoder merges information from the style guidance image, LR image, and

vector map, thus generating a conditional feature map encapsulating semantic and style information. Lastly, the adapter translates this conditional feature into multi-scale features compatible with the U-Net network architecture. These features are then element-wise added to the encoding and decoding layers of the U-Net, ensuring effective feature fusion and guidance during the generation process.

3.3. Content-style encoder

To efficiently fuse content information from vector maps and inject style information from style guidance images into LR images, a multi-branch content-style encoder (CS-Encoder) is designed, whose detailed structure is shown in Fig. 4. It consists two key components: the content guided module (CGM) and the style correction module (SCM), which together produce a conditional feature with semantic information and style information.

3.3.1 Content guided module

In the content guidance module, we integrate semantic information from vector maps into LR images at multiple scales. In the first branch, multi-scale features of the vector map are extracted through convolution and downsample blocks. In another branch, multi-scale features of the LR image are extracted through the basic blocks. To fuse these features, we employ spatially-adaptive denormalization (SPADE) [34] modules at each scale. The network structures of the basic block, convolution block, downsample block, and SPADE block are illustrated in Fig. 5. It is worth noting that in our design, the input of SPADE block is the feature map of LR images, which possesses very coarse texture and structural information. Consequently, our adaptation of the SPADE module differs from the original one by using both LR features and vector map features to calculate the scale factor γ and bias term β . This enables more flexibility and higher-fidelity fusion of content guidance information into LR image features. The entire process is described by the following equation:

$$\gamma^i = \text{Conv}_\gamma (\text{Conv}_{\text{share}} ([F_{\text{lr}}^i, F_{\text{map}}^i])) \quad (8)$$

$$\beta^i = \text{Conv}_\beta (\text{Conv}_{\text{share}} ([F_{\text{lr}}^i, F_{\text{map}}^i])) \quad (9)$$

$$F_{\text{lr}}^{i+1} = \gamma^i \frac{F_{\text{lr}}^i - \mu^i}{\sigma^i} + \beta^i \quad (10)$$

where F_{lr}^i and F_{map}^i represent the i -th layer of the LR image and the vector map features. $\text{Conv}_{\text{share}}$ represents the shared convolution module, while Conv_γ and Conv_β represent convolution layers used to respectively predict scale factor γ^i and bias β^i . γ^i and β^i represent the spatially variant scale factor and bias for the i -th layer, while μ^i and σ^i represent the mean and standard deviation of all input features for the i -th layer within a mini-batch. By employ-

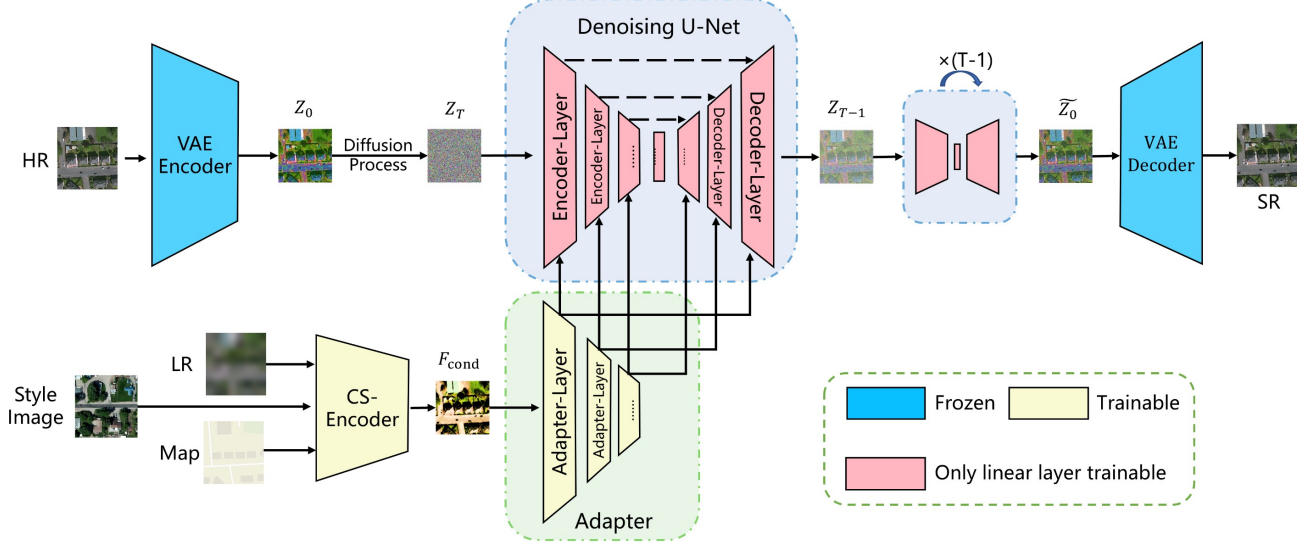


Figure 3. The framework of SGDM. A VAE is used to shift the diffusion process and reverse process from the pixel space to the latent space. During training, the latent features z_0 of HR are transformed into z_t through the diffusion process, which is then denoised through a U-Net network. To guide the denoising process, we design two modules: the content-style encoder (CS-Encoder) and the adapter. The former integrates information from LR, vector maps, and style guidance images to generate conditional features F_{cond} . The latter generates multi-scale features based on F_{cond} and performs element-wise addition with the output of the corresponding layers in the U-Net.

ing stacked content guided modules, the content information from the vector map is progressively integrated into LR features, resulting in more semantically accurate reconstructions.

3.3.2 Style correction module

To overcome the style gap between LR and HR images during model training, we propose a simple yet effective style correction module (SCM). Drawing inspiration from style transfer tasks, our approach entails extracting style features with a lightweight style encoder, followed by the application of adaptive instance normalization (AdaIN) [14], as depicted in Fig. 6. The AdaIN process can be mathematically represented as:

$$\text{AdaIN}(F_{\text{lr}}, F_{\text{sty}}) = \sigma(F_{\text{sty}}) \left(\frac{F_{\text{lr}} - \mu(F_{\text{lr}})}{\sigma(F_{\text{lr}})} \right) + \mu(F_{\text{sty}}) \quad (11)$$

Here, F_{lr} represents the output of the content guided module, while F_{sty} represents the feature maps obtained by passing the style guidance image through the style encoder. $\mu(F_{\text{lr}})$, $\sigma(F_{\text{lr}})$, $\mu(F_{\text{sty}})$, and $\sigma(F_{\text{sty}})$ represent the mean and standard deviation computed across spatial dimensions independently for each channel and each sample. Numerous style transfer studies emphasize that channel-wise statistical features in image feature maps carry crucial style information [23, 44]. During training, we use HR images as style guidance, enabling the AdaIN module to incorporate HR image style into the reconstruction, thus enhancing content

consistency learning and addressing the style discrepancy between LR and HR in real-world scenarios. During testing, any HR remote sensing images can be used as style guidance.

However, in real-world scenarios, obtaining effective style guidance images may be tedious. In such case, we resort to style sampling to obtain plausible stylized super-resolution results. Our proposed style correction module (SCM) not only supports style guidance but also facilitates style sampling. After training the entire model, we utilize the trained style encoder network to recompute the style vectors $\mu(F_{\text{hr}})$ and $\sigma(F_{\text{hr}})$ for all HR images in the training set. We then employ a normalizing flow model to model the probability distributions of these vectors separately (which corresponds directly to the term ‘HR style space’ depicted in Fig. 2). The style normalizing flow (SFlow) model, as illustrated in Fig. 6, utilizes stacked affine coupling modules [6] to map input samples conforming to arbitrary complex probability distributions into standard Gaussian distributions. SFlow can be trained efficiently with exact log-likelihood estimation and enables random style sampling during testing, thus allowing for obtaining diverse plausible super-resolution results even without explicit style guidance images.

3.4. Adapter design

CS-Encoder can sufficiently integrate coarse texture and structural features from LR images with content features from vector maps and style information from style guidance

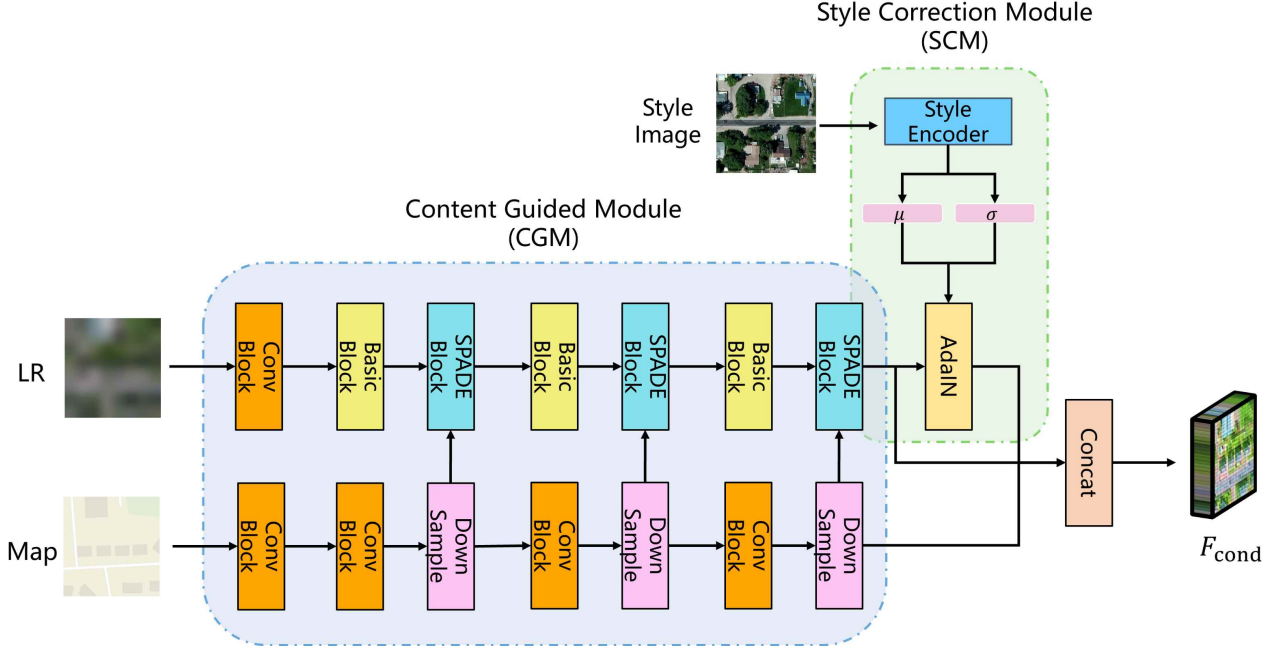


Figure 4. Detailed structure of the proposed Content-Style Encoder (CS-Encoder). It can utilize the content information from the vector map at multiple scales through the SPADE module, and achieve style injection through the AdaIN module, which results in a conditional feature F_{cond} . This feature encapsulates semantic information and style attributes.

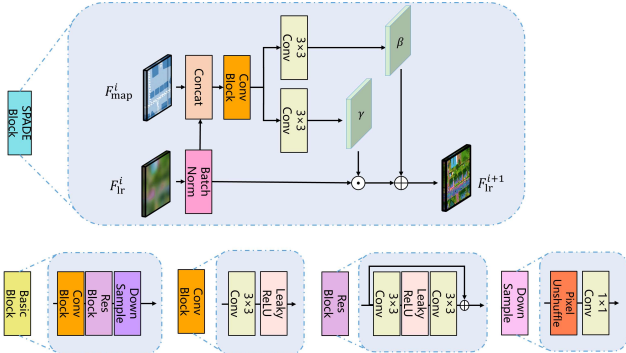


Figure 5. Structures of SPADE block, basic block and downsample block in our work.

images, ultimately producing a conditional feature F_{cond} . Since F_{cond} already contains most of the external information required for super-resolution, the role of the adapter is merely to generate multi-scale features and align them with the prior knowledge of the pre-trained Stable Diffusion model.

Therefore, the structure of the adapter module in Fig. 3 is relatively simple and it mainly consists of stacked convolution layers, residual blocks, and downsample blocks. The adapter module progressively increases the channel number of the feature maps while reducing their spatial sizes, thereby generating three different-sized conditional

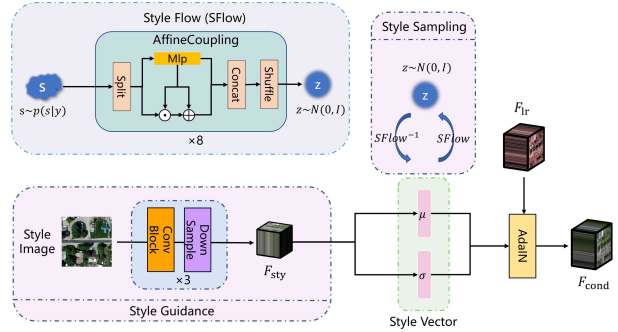


Figure 6. Structure of style correction module (SCM) proposed by us. It can achieve style guidance or style sampling through the style encoder or normalization flow respectively.

features. These features are then added element-wise to the output of each layer of the U-Net network for guiding the generation process of the Stable Diffusion model.

3.5. Loss function

The training process of the Semantic Guided Diffusion Model (SGDM) comprises two stages. The first stage corresponds to training the SGDM, whereas the second stage corresponds to training the SFlow model. The trainable parameters of the first stage are indicated in Fig. 3, and the

loss function is as follows:

$$L = \mathbb{E}_{(z_0, \epsilon, lr, map, t)} \|\epsilon - \epsilon_\theta(z_t, t, lr, map)\|^2 \quad (12)$$

where lr and map denotes the input LR images and vector maps, ϵ refers to randomly sampled Gaussian noise, t represents an integer timestamp sampled from the interval $[0, T]$ and ϵ_θ is the denoising U-Net model.

After completing the first stage of training, we can recompute the style vectors $\mu(F_{lr})$ and $\sigma(F_{lr})$ for HR images in the training dataset and model their probability distributions using SFlow. The normalization flow model aims to establish a bijective mapping from an arbitrary distribution to a easy-to-sample distribution (such as the standard Gaussian distribution) through a series of chained invertible networks. Therefore, negative log-likelihood (NLL) can be used as the loss function to optimize it. Taking μ as an example, assuming h_k represents the output of the k -th affine coupling layer f_θ^k , and h_0 and h_N represent the original input μ and the output random variable z , then the loss function of SFlow can be expressed as:

$$\begin{aligned} \text{NLL} = -\log p(\mu) &= \frac{D}{2} \log(2\pi) + \frac{1}{2} \|f_\theta(\mu)\|^2 \\ &- \sum_{k=1}^N \log \left| \text{Det} \frac{\partial f_\theta^k(h^{k-1})}{\partial h^{k-1}} \right| \end{aligned} \quad (13)$$

where f_θ represents the forward process of SFlow.

4. Datasets and image quality assessment metrics

4.1. Datasets

In this paper, we collect a new benchmark dataset named Cross-Modal Super-Resolution Dataset (CMSRD) to validate the proposed SGDM and hope to facilitate future research on large scale factor remote sensing image super-resolution. This dataset is composed of two parts: synthetic data and real-world data, with detailed information depicted in Table 1 and some examples of the image pairs shown in Fig. 7.

The CMSRD consists of triplets LR-Map-HR, all HR images are sourced from World Imagery, while all vector maps are obtained from Open Street Map. The synthetic dataset comprises 45,300 image pairs, with 45,000 pairs used for training and 300 pairs for testing. LR images are obtained by downsampling HR images by a factor of 32 using bicubic interpolation. The synthetic dataset is used to validate the effectiveness of introducing vector maps in large scale factor remote sensing image super-resolution. The real-world dataset consists of 50,754 image pairs, with 50,364 used for training and 390 for testing. In contrast to the synthetic dataset, LR images in the real-world dataset are sourced from the Sentinel-2 satellite series. We ensure

16× spatial size difference between HR and LR through bicubic resampling. As shown in Fig. 7, there exists content consistency and style gap among remote sensing images from different sources, which is one of the main issues to be explored in this work.

4.2. Image quality assessment metrics

To conduct a comprehensive evaluation of various remote sensing image super-resolution methods, we employ both full-reference and no-reference image quality assessment metrics. For assessing reconstruction fidelity, peak signal noise ratio (PSNR) and structure similarity (SSIM) [52] calculated on the Y channel of the YCbCr color space are used. For the perceptual quality evaluation, full-reference metrics learned perceptual image patch similarity (LPIPS) [65] and deep image structure and texture similarity (DISTS) [5] are employed. Furthermore, fréchet inception distance (FID) [12] is used to gauge the distributional disparity between the ground truth images and the SR images. For no-reference image quality assessment, we use metrics such as multi-scale image quality transformer (MUSIQ) [18] and CLIP-IQA [48].

5. Experiments

5.1. Implementation details

Our SGDM is built based upon the Stable Diffusion 2.1-base model. We implement the proposed SGDM using the PyTorch framework and all experiments are conducted on two NVIDIA GeForce RTX 3090 GPUs.

The training phase consists of two stages. Firstly, we fine-tune the Stable Diffusion model using the loss function in Equation 12. During this phase, we optimize the parameters of content-style encoder, adapter, and the linear layers of U-net, which amounts to a total of 148M trainable parameters. We train the model with a batch size of 32 for 150K steps, and employ the AdamW optimizer with a learning rate of 5×10^{-5} . Subsequently, we utilize the trained style encoder to re-calculate style vectors (μ and σ) for all HR images in the training set and use them to train the SFlow model. The SFlow architecture follows the structure proposed in [6], with hidden layer dimensions set to 16, 32, 32, 64 and the number of affine coupling layers set to 8. We employ two separate SFlow models for the distributions of μ and σ . We use the Adam optimizer with a learning rate of 4×10^{-4} , and the training of SFlow can be completed within two hours.

It is important to note that our style correction module (SCM), designed as a plug-and-play module, is not required when experimenting on synthetic datasets (referred to as SGDM). However, for real-world datasets, we integrate the SCM to address the style discrepancies between LR and HR images (referred to as SGDM+). Considering that previous

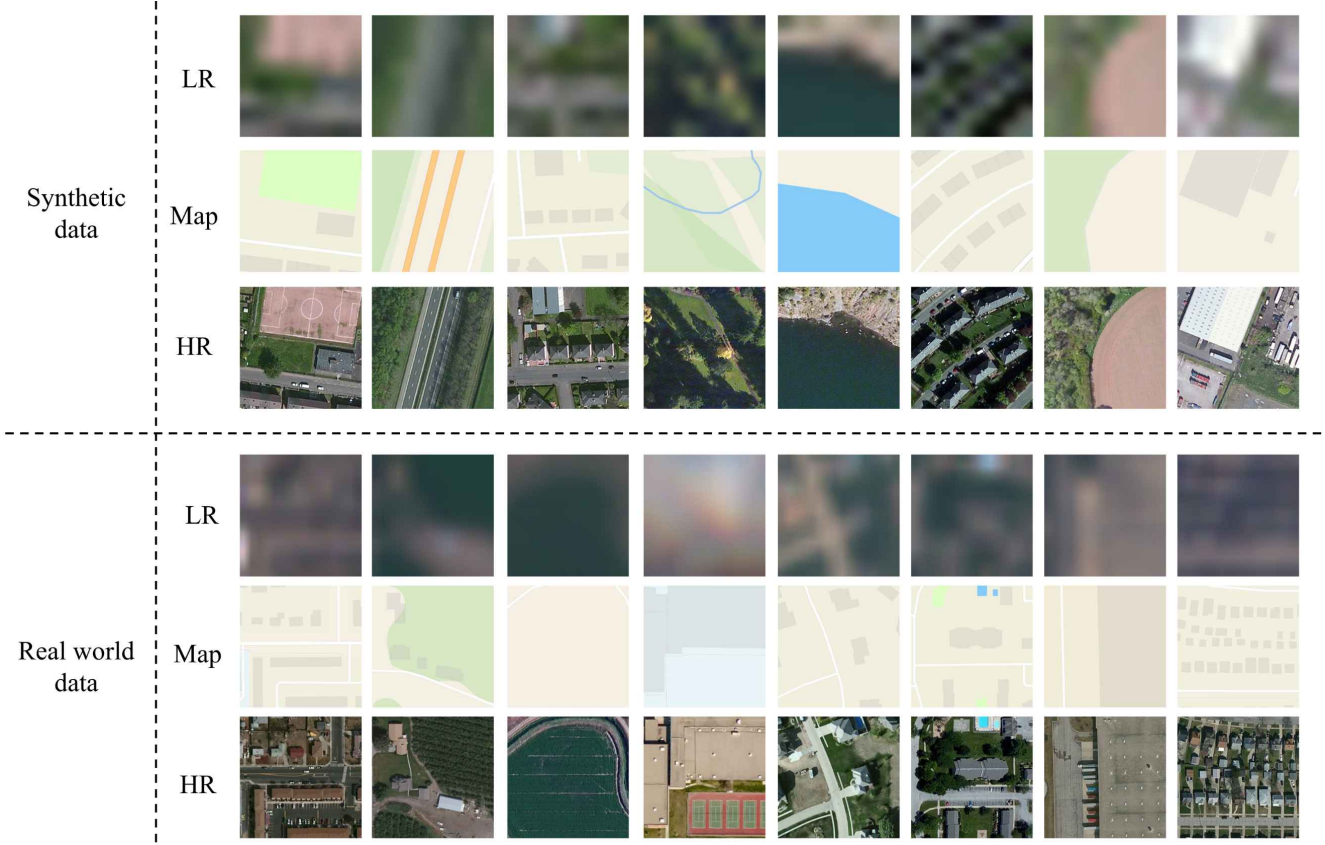


Figure 7. Examples of LR-Map-HR pairs in the CMSRD dataset. The dataset covers a wide range of scenes, including forests, rivers, streets, residential areas, industrial areas, water bodies, squares, and so on.

Table 1. Detailed information about the CMSRD.

Type	Dataset	Image pair number	HR source	LR source	Vector map source	Resolution of HR	Resolution of LR
Synthetic	Training set	45000	World Imagery	Bicubic down	OSM	1.07 m	34.24 m
	Testing set	300	World Imagery	Bicubic down	OSM	1.07 m	34.24 m
Real world	Training set	50364	World Imagery	Sentinel-2	OSM	1.07 m	10 m
	Testing set	390	World Imagery	Sentinel-2	OSM	1.07 m	10 m

methods for large scale factor super-resolution are only suitable for specific types of scenes, such as face [4, 11, 33], here, we select some state-of-the-art (SOTA) SR methods for natural images to do the comparison, such as ESRGAN [50], SwinIR [24] and ResShift[62]. LDM [36] is also chosen as a comparison method to validate the effectiveness of the semantic and style guidance we proposed. In addition, we also select two SOTA methods for remote sensing image super-resolution for comparison, *i.e.*, the EDiffSR [53] and TTST [54]. For the sake of fairness, all methods are trained on our CMSRD dataset using the source code and hyper-parameter settings provided by those papers. It should be noted that the original hyper-parameter settings

of ESRGAN results in convergence issues in scenarios of large scale factor super-resolution. Therefore, we adjust the scale of its loss functions to make it better suited for this task.

5.2. Experiments on synthetic data

5.2.1 Quantitative SR results

Table 2 presents $32\times$ SR results of different methods compared on synthetic data. Transformer-based regression models, such as SwinIR and TTST, exhibit the highest PSNR and SSIM scores. However, these methods often produce over smooth SR images, which negatively impacts perceptual quality, as reflected by the low LPIPS, DISTs,

Table 2. Quantitative comparisons with different methods on the synthetic data for $32\times$ SR and real-world data for $16\times$ SR, where the bold font indicates the best performance. The symbols \uparrow and \downarrow respectively represent that higher or lower values indicate better performance.

Type	Metric	ESRGAN	SwinIR	LDM	ResShift	TTST	EDiffSR	SGDM/SGDM+
Synthetic	PSNR \uparrow	20.26	21.74	20.12	19.29	21.88	20.32	20.65
	SSIM \uparrow	0.3233	0.4029	0.3121	0.3021	0.4064	0.2836	0.3338
	LPIPS \downarrow	0.4551	0.8932	0.4925	0.4585	0.8396	0.4517	0.4344
	DISTS \downarrow	0.2561	0.5528	0.2609	0.2537	0.5001	0.2480	0.2356
	FID \downarrow	70.67	357.8	42.43	86.24	295.3	108.3	36.62
	MUSIQ \uparrow	38.13	19.99	39.40	37.31	17.77	38.54	40.30
	CLIQQA \uparrow	0.5951	0.2683	0.6116	0.4546	0.2471	0.4590	0.6238
Real world	LPIPS \downarrow	0.5592	0.9137	0.6006	0.6218	0.9108	0.6064	0.5978
	DISTS \downarrow	0.3124	0.5948	0.3225	0.3516	0.5615	0.3458	0.3231
	FID \downarrow	98.15	423.2	49.40	166.4	359.7	156.1	44.81
	MUSIQ \uparrow	44.23	20.51	46.70	44.41	19.11	42.21	48.92
	CLIQQA \uparrow	0.4727	0.2581	0.5956	0.3989	0.2547	0.4385	0.6064

FID, MUSIQ, and CLIQQA scores. Meanwhile, ESRGAN, ResShift, and EDiffSR, as generative models based on GAN, diffusion, and SDE, exhibit similar performance. They show improved perceptual quality but still struggle for maintaining fidelity, leading to lower PSNR and SSIM. However, our proposed SGDM outperforms in both aspects and achieves the best balance between perceptual quality and fidelity. In addition to achieving the best performance across all perceptual metrics, SGDM also achieves relatively high PSNR and SSIM scores. On one hand, SGDM can utilize coarse texture and structural information from LR images and explicit semantic information from vector maps to effectively improve the fidelity of the reconstruction results; on the other hand, by leveraging the powerful generative prior of the Stable Diffusion, SGDM is still able to recover detailed textures that match real scenes even in extreme large factor super-resolution scenarios. Notably, despite relatively good perceptual metrics of LDM, it has a significantly higher number of trainable parameters (865M) compared to SGDM (148M), which highlights the efficiency and effectiveness of our network architecture.

5.2.2 Qualitative SR results

In Fig. 8, we present a visual comparison of super-resolution results using different methods on the synthetic dataset. Due to the low spatial resolution of the LR input, a substantial amount of high-frequency information is lost and there exhibit significant semantic ambiguity. Consequently, traditional transformer-based regression models (SwinIR and TTST) can only produce overly smooth results, struggling to recover the lost high-frequency texture details. Among generative methods, ESRGAN and ResShift perform relatively better. ESRGAN can recover most of the high-frequency details, but suffer from serious distortion and deformation of the reconstructed ground ob-

jects. In contrast to ESRGAN, ResShift can reconstruct more regular shapes of objects, but it cannot recover as much high-frequency details as ESRGAN. LDM can generate richer and more realistic details compared to ESRGAN and ResShift. However, due to the lack of semantic guidance, positions and shapes of the generated objects exhibit some disarray. Thanks to the precise semantic guidance provided by vector maps and the powerful generative capabilities of Stable Diffusion, the proposed SGDM effectively addresses the problem of semantic ambiguity and the loss of high-frequency details, thereby achieving reconstruction results that balance realism and fidelity.

5.3. Experiments on real-world data

5.3.1 Quantitative SR results

Table 2 shows the evaluation results of different comparative methods on real-world data for $16\times$ SR. Our proposed SGDM+ achieves the best performance on all no-reference metrics. However, it lags slightly behind ESRGAN in two full-reference perceptual metrics. This is because during testing, we do not provide any style guidance images and instead get completely random style vectors by sampling from the latent space of SFlow. Therefore, one-to-one evaluation metrics cannot fully demonstrate the advantages of SGDM+. However, the lower FID indicates that SGDM+ can better capture the distribution of HR images compared to other methods. This is because SGDM+ can independently model the style of HR through the SCM module, effectively overcoming the style misalignment between LR and HR in real-world scenarios.

5.3.2 Qualitative SR results

Visual comparisons between different methods on real-world data are shown in Fig. 9. Due to the entanglement

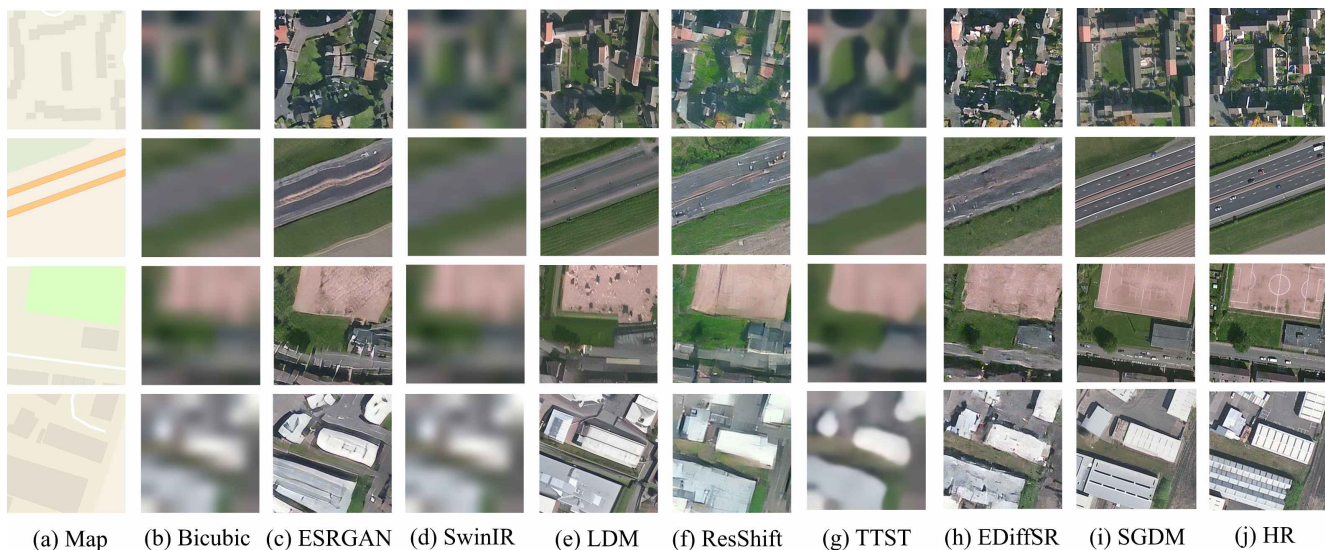


Figure 8. Visual comparison of $32\times$ super-resolution on synthetic dataset. We select four representative scenes: residential areas, roads, squares, and factories.



Figure 9. Visual comparison of $16\times$ super-resolution on real-world dataset.

between content attributes and style attributes, the results provided by all comparative methods tend to have the average style of HR images, for example SR images tend to be darker. SGDM+ can perform style sampling based on the normalizing flow model, forming a more flexible solution space. Additionally, we find that due to the style differences between LR and HR in real-world datasets, some comparative methods even have difficulty converging during training (such as ResShift and EDiffSR), resulting in severely distorted SR results. ESRGAN, while capable of producing relatively accurate ground objects, falls short in

generating rich textures. While LDM can generate results with higher realism, it often generates ground objects that do not match the ground truth due to the lack of accurate semantic guidance. SGDM+, on the other hand, obtains SR results that combine fidelity and realism under the guidance of vector maps and the support of pre-trained Stable Diffusion model.



Figure 10. Visual comparison between reconstruction results given different style guidance images.



Figure 11. Visual comparison between reconstruction results with different sampling seeds for normalizing flow.

5.3.3 SR results of different style control strategies

Style guidance from example HR image. In many instances, addressing remote sensing image super-resolution often involves leveraging heterogeneous or historical remote sensing images as references. For example, [8] proposed using HR remote sensing images captured by other satellite platforms as references to assist in the super-resolution process, thereby obtaining more realistic texture details. In contrast to their content-based reference methods, we advocate using HR remote sensing images as a style reference to overcome the style misalignment between LR and HR images. During inference, our framework can reuse the trained style encoder to extract the style vectors of the style guidance images, and then apply style injection on the LR feature maps through the AdaIN module. As shown in Fig. 10, when providing different style guidance images, the model can perform instance-level style guidance (such as colors of buildings and roads, and the density of ve-

getation), thereby obtaining more controllable reconstruction results.

Style sampled from fitted probabilistic distribution.

In the most challenging scenario where no style guidance images are available, we can directly sample from the SFlow to acquire style vectors for super-resolution. It should be noted that due to the limited training data, the normalizing flow model can only approximate (rather than fully simulate) the style distribution of HR images. Therefore, compared to style guidance, style sampling will lower the quality and increase the uncertainty of the reconstruction results. As shown in Fig. 11, by changing the random seed for sampling from the style normalizing flow, we can obtain reconstruction results that are consistent in content but diverse in style. Due to the lack of appropriate style guidance, these results represent the lower bound of the performance of SGDM+ under extreme conditions (which is also the performance of SGDM+ recorded in Table 2).

Table 3. Ablation study of our method (SGDM) on the synthetic split of CMSRD.

LR condition	Vector map prior	Stable Diffusion prior	SPADE block	LPIPS ↓	FID ↓
✓	✓	×	✓	0.8498	277.2
✓	×	✓	×	0.4652	42.43
✓	✓	✓	×	0.4478	43.83
✓	✓	✓	✓	0.4344	36.63

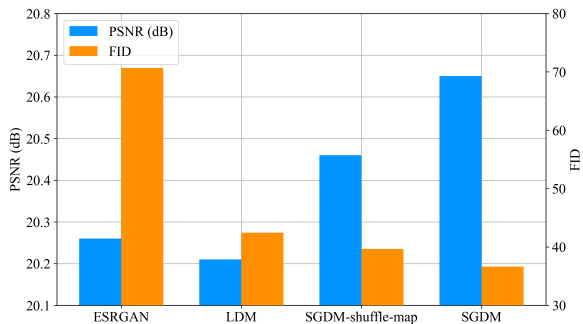


Figure 12. Performance of different methods on the synthetic dataset. ‘SGDM-shuffle-map’ represents using vector maps completely unrelated to ground truth.

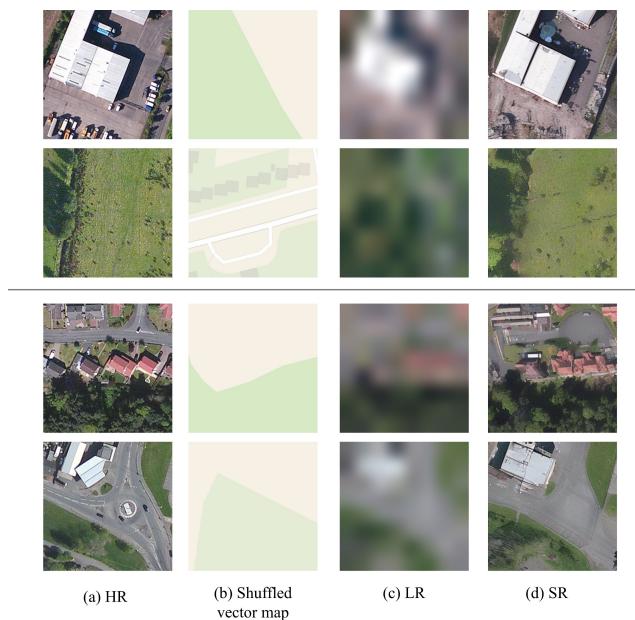


Figure 13. Visualization of the reconstruction results of SGDM given vector map as semantic guidance. The reconstruction results of the first two rows are less affected by vector maps, while the last two rows are more significantly influenced.

6. Ablation studies

6.1. Effectiveness of diffusion prior

The powerful generative capabilities of pre-trained Stable Diffusion can significantly enhance the visual quality of reconstruction outcomes. To assess its efficacy, we conduct an experiment where we employ our proposed content guided module (CGM) alone, bypassing the pre-trained Stable Diffusion as a prior. As demonstrated in the first row of Table 3, the absence of the pre-trained Stable Diffusion prior leads to significantly lower perceptual quality in the reconstruction, due to the inherent limitations of traditional regression models in bridging the substantial spatial resolution disparity between LR and HR images.

6.2. Effectiveness of semantic guidance

For our proposed SGDM, vector maps serve as semantic guidance to enhance the fidelity of the reconstruction results. We evaluate the effectiveness of vector maps from two perspectives: whether vector maps are useful for improving the results, and whether the method we introduce vector maps is the most effective. For the former, we use only LR as the condition to guide the generation process of the diffusion model. For the latter, we eliminate all SPADE modules in the content guided module and simply merge the features of LR and the vector map by concatenation. The results of these experiments are presented in the second and third rows of Table 3. These experiments demonstrate that incorporating vector maps through concatenation can also improve reconstruction fidelity. The SPADE module, as a spatially adaptive feature modulation technique, exploits the full potential of the semantic information from vector maps, thus yielding better results compared to simple concatenation.

Additionally, we also conduct some experiments to test the robustness of SGDM. By inputting vector maps that are entirely unrelated to the ground truth, we can assess the reliance of the model on vector maps. As depicted in Fig. 12, even with irrelevant vector maps, SGDM still generates relatively plausible reconstructions, outperforming LDM and ESRGAN. Conversely, when vector maps lack accurate semantic guidance, performance of the SGDM decreases, indicating the efficacy of vector map integration. From Fig. 13, it can be observed that the reconstruction results of some remote sensing images, such as large scale buildings and

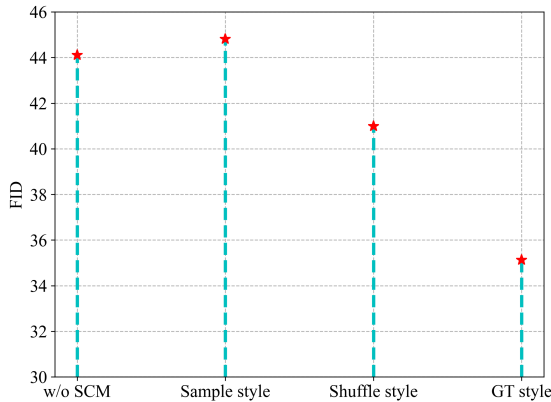


Figure 14. Performance of SGDM+ under different style guidance strategies. ‘Sample style’ refers to style sampling through normalization flows. ‘Shuffle style’ denotes style guidance using randomly chosen HR images. ‘GT style’ indicates directly using the ground truth for style guidance.

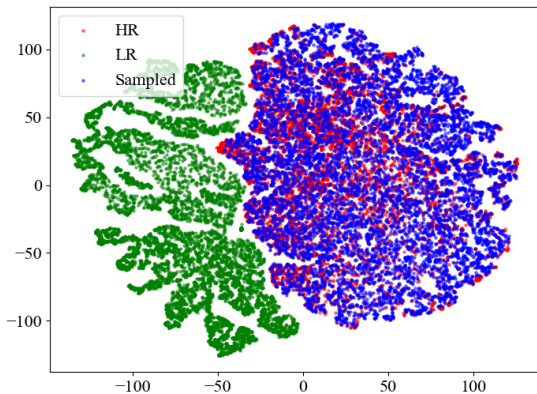


Figure 15. The t-SNE visualization of style vectors. It can be observed that there is a clear distribution difference between LR and HR, while our style normalization flow fits well into the style distribution of HR.

cluttered texture areas, are not affected by the inaccurate semantic guidance from the vector maps. However, for dense urban scenes, the model heavily relies on semantic information provided by vector map, thereby leading to less satisfactory results.

6.3. Effectiveness of style modelling

To tackle the issue of style inconsistency between LR and HR images in real-world scenarios, we’ve developed a style correction module to enhance the capability of the model for style modelling. During testing, we can either employ

the style encoder for style guidance or utilize normalization flow for random style sampling. Therefore, theoretically, completely random style sampling and using the ground truth for style guidance respectively represent the lower and upper bounds of the performance of SGDM+. Additionally, we can input randomly selected HR images for style guidance, which represents the average performance of SGDM+ under general conditions. We conduct these three inference methods separately and compare the results with the approach of not using the style correction module (*i.e.*, SGDM). The obtained results are shown in Fig. 14. It can be observed that using the ground truth as style guidance and random style sampling achieve the best and worst reconstruction results. Notably, using randomly selected HR images for style guidance also produces favorable results, surpassing the model without the style correction module. These findings robustly attest to the efficacy and substantial practical applications of our proposed style correction module.

To visually inspect the distinct style distributions between LR and HR, we present a visualization of style vectors for 10,000 randomly chosen training pairs in Fig. 15. The comparison clearly illustrates a substantial difference in style distribution between HR and LR (denoted as ‘HR style space’ and ‘LR style space’ in Fig. 2). Our proposed style normalization flow effectively aligns with the HR image style distribution. During testing, by directly sampling from the normalization flow, we can provide useful style priors to the model, thereby enhancing the reconstruction fidelity.

6.4. Evaluate usability of SR images on downstream vision tasks

The evaluation of natural image quality primarily relies on quantitative metrics and visual appeal. However, the value of remote sensing images lies in their performance on relevant analysis tasks. To assess the reconstruction quality of various SR methods comprehensively, we choose two representative downstream tasks (scene recognition and semantic segmentation) to showcase the superiority of our proposed method in perceptual quality. Due to the absence of the ground truth, we leverage a pre-trained remote sensing foundation model (RVSA [46]) with strong generalization capabilities to analyze the SR results. Our focus is on the relative performance of SR results compared to HR images in the context of these tasks, not the absolute accuracy of SR results. Thus all metrics, such as classification accuracy and mean intersection over union (mIoU), are computed using HR analysis results as a reference.

Scene recognition. The scene recognition task aims to classify input remote sensing images, enabling a comprehensive assessment of global semantic consistency between SR results and HR. We employ the RVSA model fine-tuned

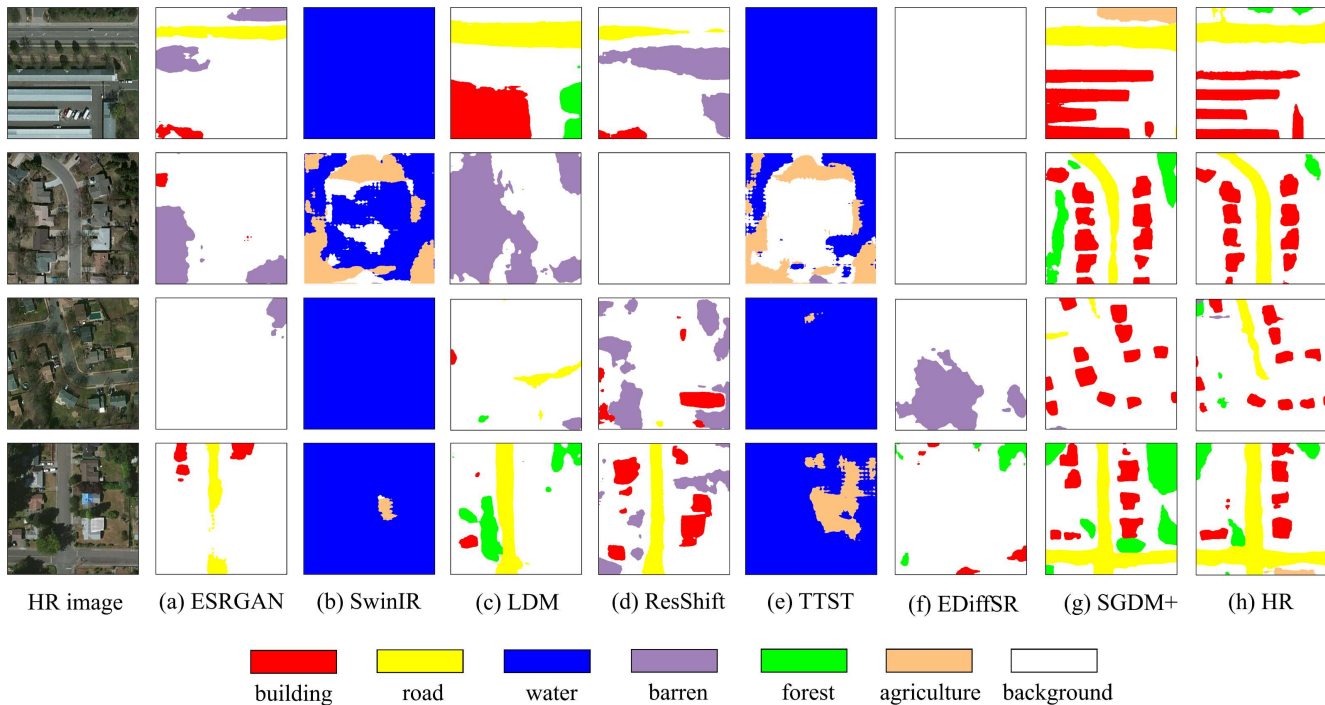


Figure 16. Visual comparison of semantic segmentation results from different super-resolution methods.

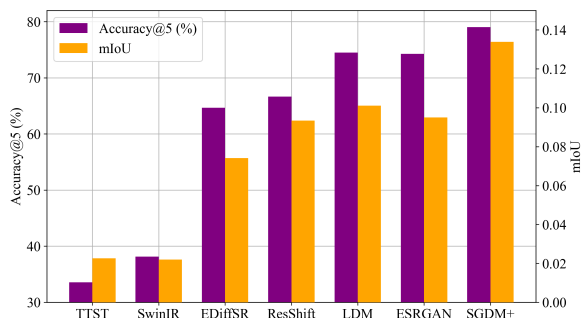


Figure 17. Quantitative comparison of scene recognition and semantic segmentation results among different super-resolution methods.

on the UC Merced Land-Use dataset [59] to classify the test set images in the real-world CMSRD dataset. As shown in Fig. 17, our proposed SGDM+ achieves the highest classification accuracy (*i.e.*, the most similar classification results compared to HR), with a top-5 accuracy close to 80%. This indicates that the SR results of SGDM+ have the highest fidelity for machine perception. Notably, all generative models, including SGDM+, outperform regression models like TTST and SwinIR, highlighting the limitations of pixel-level loss for machine vision tasks.

Semantic segmentation. The semantic segmentation task aims to classify each pixel of a given remote sensing image. We utilize this task to evaluate the consistency between SR results and HR in terms of local semantics. We use the RVSA model fine-tuned on the LoveDA dataset [47] to segment the test images, and the mean intersection over union (mIoU) of segmentation results is displayed in Fig. 17. Consistent with scene recognition, SGDM+ delivers the best segmentation outcomes, significantly outperforming other methods. In Fig. 16, visual comparisons reveal that most comparative methods struggle with precise ground object reconstruction, while SGDM+ provides the closest results to HR, particularly for buildings and roads, underscoring the promising prospects of our proposed method.

7. Conclusion

In this paper, we propose a novel framework (SGDM) for large scale factor remote sensing image super-resolution. To address challenges such as semantic inaccuracies and texture blurriness commonly encountered in this task, we utilize vector maps to provide semantic guidance and exploit the powerful generative capabilities of the pre-trained Stable Diffusion model to generate more realistic SR images. Additionally, considering the style differences between LR and HR caused by the sensor-specific imaging characteristics in real-world scenarios, we develop a method for extracting style information and modeling its probability dis-

tribution. During testing, diverse outputs can be obtained through style guidance or style sampling.

Extensive experiments are conducted on our proposed CMSRD dataset. Both qualitative and quantitative experiments demonstrate the superiority of our proposed framework. Comprehensive ablation experiments validate the necessity of key components in SGDM, including vector maps, generative priors, and style correction module. Finally, we further demonstrate the application prospects of our proposed framework through two downstream tasks: scene recognition and semantic segmentation. In future work, we will further explore the feasibility of large scale factor remote sensing image super-resolution by introducing richer explicit priors (such as digital elevation maps, historical remote sensing images, etc.) and higher-quality generative priors (such as pre-trained models for remote sensing images).

References

- [1] CCG Bamford, N Kelly, L Dalla Rosa, DE Cade, PT Fretwell, PN Trathan, HC Cubaynes, AFC Mesquita, L Gerish, AS Friedlaender, et al. A comparison of baleen whale density estimates derived from overlapping satellite imagery and a shipborne survey. *Scientific reports*, 10(1):12985, 2020. [1](#)
- [2] Marcel C Buhler, Andrés Romero, and Radu Timofte. Deepsee: Deep disentangled semantic explorative extreme super-resolution. In *Proceedings of the Asian Conference on Computer Vision*, 2020. [3](#)
- [3] Adrian Bulat and Georgios Tzimiropoulos. Super-fan: Integrated facial landmark localization and super-resolution of real-world low resolution faces in arbitrary poses with gans. In *Proceedings of the IEEE conference on computer vision and pattern recognition*, pages 109–117, 2018. [1](#)
- [4] Kelvin CK Chan, Xintao Wang, Xiangyu Xu, Jinwei Gu, and Chen Change Loy. Glean: Generative latent bank for large-factor image super-resolution. In *Proceedings of the IEEE/CVF conference on computer vision and pattern recognition*, pages 14245–14254, 2021. [2](#), [3](#), [9](#)
- [5] Keyan Ding, Kede Ma, Shiqi Wang, and Eero P Simoncelli. Image quality assessment: Unifying structure and texture similarity. *IEEE transactions on pattern analysis and machine intelligence*, 44(5):2567–2581, 2020. [8](#)
- [6] Laurent Dinh, Jascha Sohl-Dickstein, and Samy Bengio. Density estimation using real nvp. *arXiv preprint arXiv:1605.08803*, 2016. [6](#), [8](#)
- [7] Chao Dong, Chen Change Loy, Kaiming He, and Xiaoou Tang. Image super-resolution using deep convolutional networks. *IEEE transactions on pattern analysis and machine intelligence*, 38(2):295–307, 2015. [1](#), [3](#)
- [8] Runmin Dong, Lixian Zhang, and Haohuan Fu. Rrsgan: Reference-based super-resolution for remote sensing image. *IEEE Transactions on Geoscience and Remote Sensing*, 60: 1–17, 2021. [12](#)
- [9] Runmin Dong, Shuai Yuan, Bin Luo, Mengxuan Chen, Jinxiao Zhang, Lixian Zhang, Weijia Li, Juepeng Zheng, and Haohuan Fu. Building bridges across spatial and temporal resolutions: Reference-based super-resolution via change priors and conditional diffusion model. *arXiv preprint arXiv:2403.17460*, 2024. [3](#)
- [10] William T Freeman, Thouis R Jones, and Egon C Pasztor. Example-based super-resolution. *IEEE Computer graphics and Applications*, 22(2):56–65, 2002. [1](#)
- [11] Jinjin Gu, Yujun Shen, and Bolei Zhou. Image processing using multi-code gan prior. In *Proceedings of the IEEE/CVF conference on computer vision and pattern recognition*, pages 3012–3021, 2020. [3](#), [9](#)
- [12] Martin Heusel, Hubert Ramsauer, Thomas Unterthiner, Bernhard Nessler, and Sepp Hochreiter. Gans trained by a two time-scale update rule converge to a local nash equilibrium. *Advances in neural information processing systems*, 30, 2017. [8](#)
- [13] Jonathan Ho, Ajay Jain, and Pieter Abbeel. Denoising diffusion probabilistic models. *Advances in neural information processing systems*, 33:6840–6851, 2020. [3](#)
- [14] Xun Huang and Serge Belongie. Arbitrary style transfer in real-time with adaptive instance normalization. In *Proceedings of the IEEE international conference on computer vision*, pages 1501–1510, 2017. [6](#)
- [15] Justin Johnson, Alexandre Alahi, and Li Fei-Fei. Perceptual losses for real-time style transfer and super-resolution. In *Computer Vision—ECCV 2016: 14th European Conference, Amsterdam, The Netherlands, October 11–14, 2016, Proceedings, Part II 14*, pages 694–711. Springer, 2016. [1](#)
- [16] Tero Karras, Samuli Laine, and Timo Aila. A style-based generator architecture for generative adversarial networks. In *Proceedings of the IEEE/CVF conference on computer vision and pattern recognition*, pages 4401–4410, 2019. [3](#)
- [17] Tero Karras, Samuli Laine, Miika Aittala, Janne Hellsten, Jaakko Lehtinen, and Timo Aila. Analyzing and improving the image quality of stylegan. In *Proceedings of the IEEE/CVF conference on computer vision and pattern recognition*, pages 8110–8119, 2020. [3](#)
- [18] Junjie Ke, Qifei Wang, Yilin Wang, Peyman Milanfar, and Feng Yang. Musiq: Multi-scale image quality transformer. In *Proceedings of the IEEE/CVF international conference on computer vision*, pages 5148–5157, 2021. [8](#)
- [19] Wei-Sheng Lai, Jia-Bin Huang, Narendra Ahuja, and Ming-Hsuan Yang. Deep laplacian pyramid networks for fast and accurate super-resolution. In *Proceedings of the IEEE conference on computer vision and pattern recognition*, pages 624–632, 2017. [1](#)
- [20] Christian Ledig, Lucas Theis, Ferenc Huszár, Jose Caballero, Andrew Cunningham, Alejandro Acosta, Andrew Aitken, Alykhan Tejani, Johannes Totz, Zehan Wang, et al. Photo-realistic single image super-resolution using a generative adversarial network. In *Proceedings of the IEEE conference on computer vision and pattern recognition*, pages 4681–4690, 2017. [3](#)
- [21] Ke Li, Gang Wan, Gong Cheng, Liqiu Meng, and Junwei Han. Object detection in optical remote sensing images: A survey and a new benchmark. *ISPRS journal of photogrammetry and remote sensing*, 159:296–307, 2020. [1](#)

- [22] Xin Li, Yulin Ren, Xin Jin, Cuiling Lan, Xingrui Wang, Wenjun Zeng, Xinchao Wang, and Zhibo Chen. Diffusion models for image restoration and enhancement—a comprehensive survey. *arXiv preprint arXiv:2308.09388*, 2023. 3
- [23] Yijun Li, Chen Fang, Jimei Yang, Zhaowen Wang, Xin Lu, and Ming-Hsuan Yang. Universal style transfer via feature transforms. *Advances in neural information processing systems*, 30, 2017. 6
- [24] Jingyun Liang, Jiezhong Cao, Guolei Sun, Kai Zhang, Luc Van Gool, and Radu Timofte. Swinir: Image restoration using swin transformer. In *Proceedings of the IEEE/CVF international conference on computer vision*, pages 1833–1844, 2021. 9
- [25] Jingyun Liang, Andreas Lugmayr, Kai Zhang, Martin Danelljan, Luc Van Gool, and Radu Timofte. Hierarchical conditional flow: A unified framework for image super-resolution and image rescaling. In *Proceedings of the IEEE/CVF International Conference on Computer Vision*, pages 4076–4085, 2021. 3
- [26] Liang Liao, Jing Xiao, Yan Yang, Xujie Ma, Zheng Wang, and Shin’ichi Satoh. High temporal frequency vehicle counting from low-resolution satellite images. *ISPRS Journal of Photogrammetry and Remote Sensing*, 198:45–59, 2023. 1
- [27] Lukas Liebel and Marco Körner. Single-image super resolution for multispectral remote sensing data using convolutional neural networks. *The International Archives of the Photogrammetry, Remote Sensing and Spatial Information Sciences*, 41:883–890, 2016. 3
- [28] Bee Lim, Sanghyun Son, Heewon Kim, Seungjun Nah, and Kyoung Mu Lee. Enhanced deep residual networks for single image super-resolution. In *Proceedings of the IEEE conference on computer vision and pattern recognition workshops*, pages 136–144, 2017. 1, 3
- [29] Xinqi Lin, Jingwen He, Ziyang Chen, Zhaoyang Lyu, Ben Fei, Bo Dai, Wanli Ouyang, Yu Qiao, and Chao Dong. Diffbir: Towards blind image restoration with generative diffusion prior. *arXiv preprint arXiv:2308.15070*, 2023. 2, 3
- [30] Zhi-Song Liu, Wan-Chi Siu, and Yui-Lam Chan. Photo-realistic image super-resolution via variational autoencoders. *IEEE Transactions on Circuits and Systems for Video Technology*, 31(4):1351–1365, 2021. 1
- [31] Andreas Lugmayr, Martin Danelljan, Luc Van Gool, and Radu Timofte. SrfLOW: Learning the super-resolution space with normalizing flow. In *Computer Vision—ECCV 2020: 16th European Conference, Glasgow, UK, August 23–28, 2020, Proceedings, Part V 16*, pages 715–732. Springer, 2020. 1, 3
- [32] Yapeng Meng, Wenyuan Li, Sen Lei, Zhengxia Zou, and Zhenwei Shi. Large-factor super-resolution of remote sensing images with spectra-guided generative adversarial networks. *IEEE Transactions on Geoscience and Remote Sensing*, 60:1–11, 2022. 3
- [33] Sachit Menon, Alexandru Damian, Shijia Hu, Nikhil Ravi, and Cynthia Rudin. Pulse: Self-supervised photo upsampling via latent space exploration of generative models. In *Proceedings of the IEEE/CVF conference on computer vision and pattern recognition*, pages 2437–2445, 2020. 2, 3, 9
- [34] Taesung Park, Ming-Yu Liu, Ting-Chun Wang, and Jun-Yan Zhu. Semantic image synthesis with spatially-adaptive normalization. In *Proceedings of the IEEE/CVF conference on computer vision and pattern recognition*, pages 2337–2346, 2019. 5
- [35] F Pineda, V Ayma, and C Beltran. A generative adversarial network approach for super-resolution of sentinel-2 satellite images. *The International Archives of the Photogrammetry, Remote Sensing and Spatial Information Sciences*, 43:9–14, 2020. 3
- [36] Robin Rombach, Andreas Blattmann, Dominik Lorenz, Patrick Esser, and Björn Ommer. High-resolution image synthesis with latent diffusion models. In *Proceedings of the IEEE/CVF conference on computer vision and pattern recognition*, pages 10684–10695, 2022. 3, 9
- [37] Chitwan Saharia, Jonathan Ho, William Chan, Tim Salimans, David J Fleet, and Mohammad Norouzi. Image super-resolution via iterative refinement. *IEEE Transactions on Pattern Analysis and Machine Intelligence*, 45(4):4713–4726, 2022. 1, 3
- [38] Tamar Rott Shaham, Tali Dekel, and Tomer Michaeli. Singan: Learning a generative model from a single natural image. In *Proceedings of the IEEE/CVF international conference on computer vision*, pages 4570–4580, 2019. 2
- [39] Chuanliang Sun, Yan Bian, Tao Zhou, and Jianjun Pan. Using of multi-source and multi-temporal remote sensing data improves crop-type mapping in the subtropical agriculture region. *Sensors*, 19(10):2401, 2019. 1
- [40] Jian Sun, Zongben Xu, and Heung-Yeung Shum. Image super-resolution using gradient profile prior. In *2008 IEEE conference on computer vision and pattern recognition*, pages 1–8. IEEE, 2008. 1
- [41] Wanjie Sun and Zhenzhong Chen. Learning discrete representations from reference images for large scale factor image super-resolution. *IEEE Transactions on Image Processing*, 31:1490–1503, 2022. 2, 3
- [42] Radu Timofte, Vincent De Smet, and Luc Van Gool. Anchored neighborhood regression for fast example-based super-resolution. In *Proceedings of the IEEE international conference on computer vision*, pages 1920–1927, 2013. 1
- [43] Xin-Yi Tong, Gui-Song Xia, Qikai Lu, Huanfeng Shen, Shengyang Li, Shucheng You, and Liangpei Zhang. Land-cover classification with high-resolution remote sensing images using transferable deep models. *Remote Sensing of Environment*, 237:111322, 2020. 1
- [44] Dmitry Ulyanov, Andrea Vedaldi, and Victor Lempitsky. Instance normalization: The missing ingredient for fast stylization. *arXiv preprint arXiv:1607.08022*, 2016. 6
- [45] Zander S Venter, Oscar Brousse, Igor Esau, and Fred Meier. Hyperlocal mapping of urban air temperature using remote sensing and crowdsourced weather data. *Remote Sensing of Environment*, 242:111791, 2020. 1
- [46] Di Wang, Qiming Zhang, Yufei Xu, Jing Zhang, Bo Du, Dacheng Tao, and Liangpei Zhang. Advancing plain vision transformer toward remote sensing foundation model. *IEEE Transactions on Geoscience and Remote Sensing*, 61:1–15, 2022. 14

- [47] Junjue Wang, Zhuo Zheng, Ailong Ma, Xiaoyan Lu, and Yanfei Zhong. Loveda: A remote sensing land-cover dataset for domain adaptive semantic segmentation. *arXiv preprint arXiv:2110.08733*, 2021. 15
- [48] Jianyi Wang, Kelvin CK Chan, and Chen Change Loy. Exploring clip for assessing the look and feel of images. In *Proceedings of the AAAI Conference on Artificial Intelligence*, pages 2555–2563, 2023. 8
- [49] Jianyi Wang, Zongsheng Yue, Shangchen Zhou, Kelvin CK Chan, and Chen Change Loy. Exploiting diffusion prior for real-world image super-resolution. *arXiv preprint arXiv:2305.07015*, 2023. 2, 3
- [50] Xintao Wang, Ke Yu, Shixiang Wu, Jinjin Gu, Yihao Liu, Chao Dong, Yu Qiao, and Chen Change Loy. Esrgan: Enhanced super-resolution generative adversarial networks. In *Proceedings of the European conference on computer vision (ECCV) workshops*, pages 0–0, 2018. 1, 3, 9
- [51] Yifan Wang, Federico Perazzi, Brian McWilliams, Alexander Sorkine-Hornung, Olga Sorkine-Hornung, and Christopher Schroers. A fully progressive approach to single-image super-resolution. In *Proceedings of the IEEE conference on computer vision and pattern recognition workshops*, pages 864–873, 2018. 1
- [52] Zhou Wang, Alan C Bovik, Hamid R Sheikh, and Eero P Simoncelli. Image quality assessment: from error visibility to structural similarity. *IEEE transactions on image processing*, 13(4):600–612, 2004. 8
- [53] Yi Xiao, Qiangqiang Yuan, Kui Jiang, Jiang He, Xianyu Jin, and Liangpei Zhang. Ediffsr: An efficient diffusion probabilistic model for remote sensing image super-resolution. *IEEE Transactions on Geoscience and Remote Sensing*, 2023. 9
- [54] Yi Xiao, Qiangqiang Yuan, Kui Jiang, Jiang He, Chia-Wen Lin, and Liangpei Zhang. Ttst: A top-k token selective transformer for remote sensing image super-resolution. *IEEE Transactions on Image Processing*, 2024. 9
- [55] Jianchao Yang, John Wright, Thomas S Huang, and Yi Ma. Image super-resolution via sparse representation. *IEEE transactions on image processing*, 19(11):2861–2873, 2010. 1, 2
- [56] Ling Yang, Zhilong Zhang, Yang Song, Shenda Hong, Runsheng Xu, Yue Zhao, Wentao Zhang, Bin Cui, and Ming-Hsuan Yang. Diffusion models: A comprehensive survey of methods and applications. *ACM Computing Surveys*, 56(4):1–39, 2023. 3
- [57] Tao Yang, Peiran Ren, Xuansong Xie, and Lei Zhang. Pixel-aware stable diffusion for realistic image super-resolution and personalized stylization. *arXiv preprint arXiv:2308.14469*, 2023. 2, 3
- [58] Wenhan Yang, Jiashi Feng, Jianchao Yang, Fang Zhao, Jiaying Liu, Zongming Guo, and Shuicheng Yan. Deep edge guided recurrent residual learning for image super-resolution. *IEEE Transactions on Image Processing*, 26(12):5895–5907, 2017. 3
- [59] Yi Yang and Shawn Newsam. Bag-of-visual-words and spatial extensions for land-use classification. In *Proceedings of the 18th SIGSPATIAL international conference on advances in geographic information systems*, pages 270–279, 2010. 15
- [60] Hu Ye, Jun Zhang, Sibio Liu, Xiao Han, and Wei Yang. Ip-adapter: Text compatible image prompt adapter for text-to-image diffusion models. *arXiv preprint arXiv:2308.06721*, 2023. 4
- [61] Jiadi Yin, Jinwei Dong, Nicholas AS Hamm, Zhichao Li, Jianghao Wang, Hanfa Xing, and Ping Fu. Integrating remote sensing and geospatial big data for urban land use mapping: A review. *International Journal of Applied Earth Observation and Geoinformation*, 103:102514, 2021. 1
- [62] Zongsheng Yue, Jianyi Wang, and Chen Change Loy. Resshift: Efficient diffusion model for image super-resolution by residual shifting. *Advances in Neural Information Processing Systems*, 36, 2024. 9
- [63] Kai Zhang, Jingyun Liang, Luc Van Gool, and Radu Timofte. Designing a practical degradation model for deep blind image super-resolution. In *Proceedings of the IEEE/CVF International Conference on Computer Vision*, pages 4791–4800, 2021. 3
- [64] Lvmin Zhang, Anyi Rao, and Maneesh Agrawala. Adding conditional control to text-to-image diffusion models. In *Proceedings of the IEEE/CVF International Conference on Computer Vision*, pages 3836–3847, 2023. 3
- [65] Richard Zhang, Phillip Isola, Alexei A Efros, Eli Shechtman, and Oliver Wang. The unreasonable effectiveness of deep features as a perceptual metric. In *Proceedings of the IEEE conference on computer vision and pattern recognition*, pages 586–595, 2018. 8
- [66] Shu Zhang, Qiangqiang Yuan, Jie Li, Jing Sun, and Xuguo Zhang. Scene-adaptive remote sensing image super-resolution using a multiscale attention network. *IEEE Transactions on Geoscience and Remote Sensing*, 58(7):4764–4779, 2020. 3
- [67] Yulun Zhang, Kunpeng Li, Kai Li, Lichen Wang, Bineng Zhong, and Yun Fu. Image super-resolution using very deep residual channel attention networks. In *Proceedings of the European conference on computer vision (ECCV)*, pages 286–301, 2018. 3
- [68] Yulun Zhang, Zhifei Zhang, Stephen DiVerdi, Zhaowen Wang, Jose Echevarria, and Yun Fu. Texture hallucination for large-factor painting super-resolution. In *European Conference on Computer Vision*, pages 209–225. Springer, 2020. 3
- [69] Xiang Zhu, Hossein Talebi, Xinwei Shi, Feng Yang, and Peyman Milanfar. Super-resolving commercial satellite imagery using realistic training data. In *2020 IEEE International Conference on Image Processing (ICIP)*, pages 498–502. IEEE, 2020. 3